Letters

Noise Tolerance Strategy Based on Virtual Capacitor for DC–DC Converters With Continuous Control Set Model Predictive Control

Zheng Dong, Qian Chen, Jiawang Qin, Zhenbin Zhang, *Senior Member, IEEE*, Chi K. Tse, *Fellow, IEEE*, and Yonggang Xu

***Abstract*—Noise can have a negative impact on the performance of dc–dc converters with continuous control set model predictive control (CCS-MPC). This issue is commonly encountered, making it difficult to effectively apply CCS-MPC in dc–dc converters. In this letter, we present a noise tolerance method for dc–dc converters with CCS-MPC that utilizes a virtual capacitor. This method offers a simple and effective solution to address the aforementioned problem while enhancing system robustness. To illustrate, we examine the noise generation mechanism and establish a predictive model using a dual-active-bridge converter as an example. Subsequently, we delve into the influence of noise on MPC and propose a noise tolerance method centered around the virtual capacitor. Importantly, this method does not incur additional costs, computational burden, or voltage/current ripples in the system, while preserving the inherent dynamic performance of MPC. Finally, we validate the effectiveness of the proposed method through experimental results using the TMS320F28377D as the core controller.**

***Index Terms*—Continuous control set model predictive control (CCS-MPC), dc–dc converters, dual-active-bridge (DAB) converters, noise tolerance, virtual capacitors.**

I. Introduction

MODEL predictive control (MPC) serves as an efficient control technique capable of accommodating multiple constraints. Compared with finite control set (FCS)-MPC, continuous control set (CCS)-MPC has the advantages of the continuous control quantity, flexible control quantity selection and fixed switching frequency, which is generally adopted to the dc–dc converters modulated by duty cycle and phase shift, such as buck converters and dual-active-bridge (DAB) converters [1], [2], [3], [4].

The performance of converters is primarily affected by various types of noise, including switching noise, measurement noise, and quantization noise (also known as quantization error) [5]. In a previous study [2], CCS-MPC was utilized for power decoupling in a triple-active-bridge converter. However, due to the presence of noise, the resulting phase-shift angle exhibited significant and persistent fluctuations, resulting in substantial output voltage ripple and poor control performance. While high-precision measurement sensors and high-resolution analog-to-digital converter (ADC) modules can reduce measurement noise, they come at the cost of increased expenses, and other forms of noise still persist. Another proposed approach, as outlined in [6], involves employing an *LC* low-pass filter to minimize output voltage ripple, which is suitable for CCS-MPC but slows down the dynamic response speed. In addition, digital filters can present a practical solution, but they also have a negative impact on dynamic response, leading to low-frequency oscillations in the output waveform [7]. Han et al. [8] tackled the issue of sampling noise in MPC by estimating state variables using a Kalman filter at the sampling moment, but this method imposes a higher computational burden. Notably, Xiao et al. [9] introduced a moving-discretized-control-set model-predictive-control. However, this approach involves a tradeoff between dynamic performance and noise tolerance. In summary, no existing method in CCS-MPC can simultaneously balance noise tolerance, dynamic performance, cost, and computational burden.

In order to combat the negative impact of noise interference on MPC control performance, a practical control strategy centered around the virtual capacitor is presented in this communication. The focus lies on addressing the decline in performance observed in the DAB converters. By analyzing the influence of noise on CCS-MPC, an understanding of its mechanism is gained. Subsequently, a detailed noise tolerance strategy is introduced. Notably, this method stands out for its simplicity and effectiveness, making it applicable not just to DAB converters, but also to converters employing phase-shift and duty cycle control within CCS-MPC. Lastly, the efficacy of the proposed approach is confirmed through experimental validation.

Manuscript received 21 February 2024; revised 29 March 2024; accepted 15 April 2024. Date of publication 22 April 2024; date of current version 20 June 2024. This work was supported in part by the National Natural Science Foundation of China under Grant 52277192 and in part by the Hong Kong Research Grant Council under Grant GRF 112071/21E. *(Corresponding author: Jiawang Qin.)*

Zheng Dong, Qian Chen, Jiawang Qin, and Zhenbin Zhang are with the School of Electrical Engineering, Shandong University, Jinan 250061, China (e-mail: dongzheng@sdu.edu.cn; qian.chen@mail.sdu.edu.cn; jiawang.qin@mail.sdu.edu.cn; zbz@sdu.edu.cn).

Chi K. Tse is with the Department of Electrical Engineering, City University of Hong Kong, Hong Kong (e-mail: chitse@cityu.edu.hk).

Yonggang Xu is with the Emergency Management Center of State Grid Shandong Electric Power Company, Jinan 250001, China (e-mail: 13964066107@126.com).

Color versions of one or more figures in this article are available at https://doi.org/10.1109/TPEL.2024.3392260.

Digital Object Identifier 10.1109/TPEL.2024.3392260

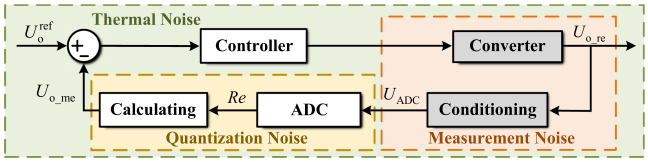

Fig. 1. Digital control diagram of the dc–dc converters.

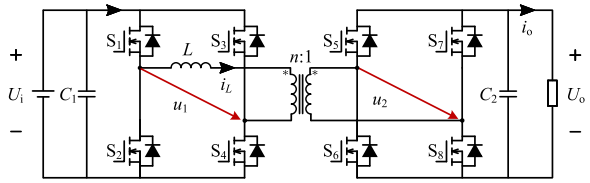

Fig. 2. Topology of a DAB converter.

II. Noise Analysis of MPC

A. Generation Sources of Noise

The digital control diagram of the dc–dc converters is depicted in Fig. 1. Influenced by the sensor's accuracy and the conditioning circuit, the measurement accuracy of the sensor is limited, at the same time, the analog component in the conditioning circuit is extremely sensitive to the change in ambient temperature and humidity. Therefore, the measurement noise will be introduced in the measurement process [5]. When conditioning the voltage U_{ADC} for analog-to-digital conversion, the limited resolution of the ADC results in quantization noise [10]. This noise occurs as the continuous electrical analog quantity is converted into a discrete digital quantity. In addition, thermal noise is inevitable due to the thermal movement of electrons in conductors. It is a natural phenomenon present in all electronic devices and transmission media. Finally, the measured output voltage $U_{\mathrm{o\_me}}$ obtained by the feedback calculation can be described as

$$\begin{cases} U_{\mathrm{o\_me}} = U_{\mathrm{o\_re}} + \Delta_u^{\mathrm{noise}} \\ \Delta_u^{\mathrm{noise}} = \Delta_u^{\mathrm{q}} + \Delta_u^{\mathrm{m}} + \Delta_u^{\mathrm{t}} \end{cases} \tag{1}$$

where $U_{\mathrm{o\_re}}$ is the actual output voltage, Δ_u^{q} is the quantization noise, Δ_u^{m} is the measurement noise, and Δ_u^{t} is the thermal noise. The above noise, collectively called ADC noise $\Delta_u^{\mathrm{niose}}$, arises out of the ADC sampling and transmission process. Assume that the ADC noise is uncorrelated between any two moments, and it can be considered as Gaussian white noise [11], [12]. According to the 3σ rule of statistics, 99.73% of the noise amplitude will be distributed within $\pm 3\sigma$.

B. MPC for the DAB Converter

The topology of a DAB converter is depicted in Fig. 2. To simplify the explanation, we will focus on the DAB converters with single phase-shift modulation. The predicted value of the output voltage can be expressed as [1]

$$U_{\mathrm{o}}(k+1) = U_{\mathrm{o}}(k) + \frac{nU_{\mathrm{i}}(k)}{2{f_{\mathrm{s}}}^2 LC_2} D(1-|D|) - \frac{I_{\mathrm{o}}(k)}{f_{\mathrm{s}} C_2}. \tag{2}$$

The control objective is to adjust the output voltage to the reference value $U_{\mathrm{o}}^{\mathrm{ref}}$ precisely, and the cost function can be constructed as

$$J = \left(U_{\mathrm{o}}(k+1) - U_{\mathrm{o}}^{\mathrm{ref}}\right)^2. \tag{3}$$

By applying CCS-MPC to minimize (3), the analytical solution can be obtained easily.

C. Mechanism of ADC Noise Effects on MPC

In this letter, we use $\Delta_{u_{\mathrm{i}}}^{\mathrm{noise}}$, $\Delta_{u_{\mathrm{o}}}^{\mathrm{noise}}$, and $\Delta_{i_{\mathrm{o}}}^{\mathrm{noise}}$ to represent the noise disturbance of the input voltage, the output voltage and the current values, respectively. Introducing the disturbance caused by ADC noise to the previously established prediction model, the output voltage prediction model shown in (2) can be transformed to

$$\begin{aligned} U_{\mathrm{o}}(k+1) = {} & U_{\mathrm{o\_re}}(k) + \Delta_{u_{\mathrm{o}}}^{\mathrm{noise}} \\ & + \frac{n\left(U_{\mathrm{i\_re}}(k) + \Delta_{u_{\mathrm{i}}}^{\mathrm{noise}}\right)}{2{f_{\mathrm{s}}}^2 LC_2} D(1-|D|) \\ & - \frac{I_{\mathrm{o\_re}}(k) + \Delta_{i_{\mathrm{o}}}^{\mathrm{noise}}}{f_{\mathrm{s}} C_2}. \end{aligned} \tag{4}$$

Based on the current working conditions, it can be observed that the values of $\Delta_{u_{\mathrm{i}}}^{\mathrm{noise}}$, $\Delta_{i_{\mathrm{o}}}^{\mathrm{noise}}$, and the voltage ripple Δu_o are significantly smaller than $\Delta_{u_{\mathrm{o}}}^{\mathrm{noise}}$. As a result, the contributions of $\Delta_{u_{\mathrm{i}}}^{\mathrm{noise}}$ and $\Delta_{i_{\mathrm{o}}}^{\mathrm{noise}}$ can be considered negligible, the specific reasons will be discussed in Section III-A. Moreover, assume the sampling value of input voltage and output current as constant values U_{i} and I_{o}.

To characterize the capability of D to regulate the output voltage, (4) can be further transformed to

$$\begin{aligned} U_{\mathrm{ad}}(k) &= U_{\mathrm{o}}(k+1) - \left(U_{\mathrm{o\_re}}(k) + \Delta_{u_{\mathrm{o}}}^{\mathrm{noise}}\right) \\ &= \frac{nU_{\mathrm{i}}}{2{f_{\mathrm{s}}}^2 LC_2} D(1-|D|) - \frac{I_{\mathrm{o}}}{f_{\mathrm{s}} C_2} \end{aligned} \tag{5}$$

where U_{ad} represents the voltage difference between two adjacent cycles in a particular D. Reconstructing the phase-shift angle function as $D_{\mathrm{sp}} = D(1-D)$, it is easy to see that D_{sp} is monotonically increasing with D being located at (0,0.5). Thus, U_{ad} is positively correlated with D_{sp}, i.e.,

$$\begin{cases} U_{\mathrm{ad\_max}} = \dfrac{nU_{\mathrm{i}}}{8{f_{\mathrm{s}}}^2 LC_2} - \dfrac{I_{\mathrm{o}}}{f_{\mathrm{s}} C_2}, & D = 0.5 \\ U_{\mathrm{ad\_min}} = -\dfrac{I_{\mathrm{o}}}{f_{\mathrm{s}} C_2}, & D = 0. \end{cases} \tag{6}$$

In steady-state operation, the value of U_{ad} is heavily influenced by the amplitude of the noise. As explained in Section II-A, if $3\sigma > U_{\mathrm{ad\_max}}$, there is a likelihood of $U_{\mathrm{ad}}(k) > U_{\mathrm{ad\_max}}$ or $U_{\mathrm{ad}}(k) < U_{\mathrm{ad\_min}}$. In such cases, the phase-shift angle D approaches the boundary values of 0.5 or 0, indicating that U_{ad} exceeds the maximum adjustable range.

To provide further clarity, Fig. 3 visually illustrates the impact of ADC noise on the system. In an ideal steady state, the output voltage will track the reference value, and D will be stable. Taking into account the random ADC noise $\Delta_u^{\mathrm{niose}}$, the actual sampled voltage is represented as $U_{\mathrm{o\_me}}$. At t_k, the actual sampled voltage $U_{\mathrm{o\_me}}$ is fed into the controller. The goal of the controller is to make $U_{\mathrm{o\_me}}$ approaching the reference voltage

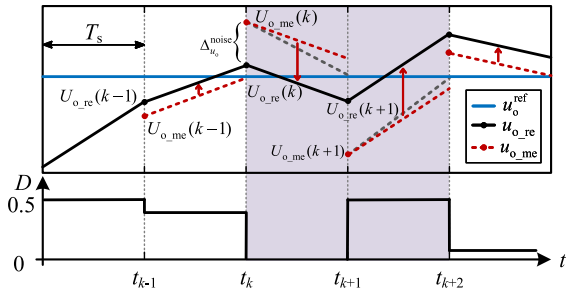

Fig. 3. Theoretical waveforms of U_o and D in ADC noise state.

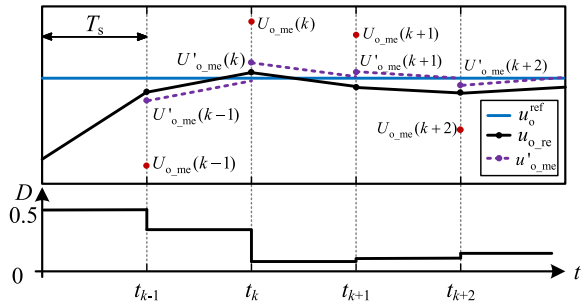

Fig. 4. Theoretical waveforms of U_o and D under virtual-capacitor-based control.

U_o^{ref}, as shown by the gray dotted line in Fig. 3. However, the regulation range of the output voltage is limited because the range of phase-shift angle is restricted. Therefore, in the interval $t_k \sim t_{k+1}$, D reaches the boundary value 0, and the variation trend of the output voltage is shown by the red dotted line in this interval. The variation of the actual output voltage U_{o_re} is shown by the black solid line, which is parallel to the red dotted line, causing U_{o_re} to deviate from U_o^{ref} at t_{k+1}. The analysis in the interval $t_{k+1} \sim t_{k+2}$ is similar to that in the interval $t_k \sim t_{k+1}$, with the difference in D reaching another boundary value 0.5. Based on the above analysis, the optimal control cannot be achieved and the phase-shift angle keeps jumping considerably, resulting in substantial fluctuations in the output voltage and the inductor current. It can be seen that the converter with CCS-MPC is characterized by poor noise tolerance, and it is of great significance to improve the robustness of CCS-MPC.

III. Virtual Capacitor Noise Tolerance Method

A. Mechanism of Noise Tolerance

To deal with the above noise problem, a simple and effective solution is proposed as follows. A virtual capacitor, constructed by the controller, is superimposed onto the real output filter capacitor in series. At this point, the output voltage prediction model becomes

$$\begin{aligned} U_o(k+1) = {} & U_{o\_re}(k) + \Delta_{u_o}^{noise} \\ & + \frac{n\left(U_{i\_re}(k) + \Delta_{u_i}^{noise}\right)}{2{f_s}^2 LC^*} D(1-|D|) \\ & - \frac{I_{o\_re}(k) + \Delta_{i_o}^{noise}}{f_s C^*} \end{aligned} \tag{7}$$

among which

$$C^* = \frac{C_2}{\beta} \tag{8}$$

where C^* represents the total capacitor and β represents the regulation coefficient of the virtual capacitor, $\beta \geq 1$. U_{ad} in (5) can be further derived as

$$\begin{aligned} U'_{ad}(k) &= \frac{\beta n U_i}{2{f_s}^2 LC_2} D(1-|D|) - \frac{\beta I_o}{f_s C_2} \\ &= \beta\left[U_o(k+1) - \left(U_{o\_re}(k) + \Delta_{u_o}^{noise}\right)\right]. \end{aligned} \tag{9}$$

To demonstrate the noise tolerance mechanism of the virtual-capacitor-based control strategy, we present the waveforms of the output voltage and phase-shift angle in Fig. 4. During the time interval $t_k \sim t_{k+1}$, the actual sampled voltage, denoted as U_{o_me}, is affected by the random ADC noise Δ_u^{niose}. To counteract this noise, the controller incorporates a regulation coefficient β using the virtual capacitor method. Consequently, the value of U'_{ad} in (9) becomes bigger than that of U_{ad} in (5). In other words, the voltage regulation range considered by the controller increases. For the same sampled voltage U_{o_me}, the controller using the virtual capacitor method no longer needs to generate a very small phase-shift angle to ensure that the output voltage at t_{k+1} tracks the reference value. Consequently, during the time interval $t_k \sim t_{k+1}$, the duty cycle D does not need to reach the boundary value, as exemplified in Fig. 4. In this case, the sampled voltage considered by the controller, denoted as U'_{o_me}, moves closer to the reference voltage. As a result, the actual output voltage U_{o_re} varies along a trajectory represented by the solid black line, which remains parallel to the dotted purple line. Comparing Fig. 3 with Fig. 4, it becomes evident that the fluctuations in the output voltage and phase-shift angle are significantly suppressed in the latter. Consequently, both the output voltage ripple and the inductor current ripple are correspondingly reduced.

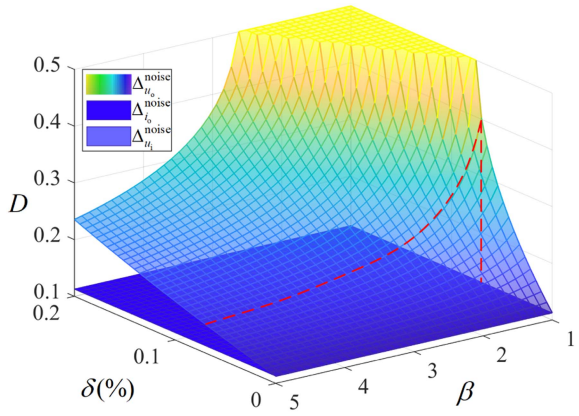

Fig. 5. Relationship between the noise intensity and β on phase-shift angle under different noise types.

The voltage noise intensity δ_u and the current noise intensity δ_i are expressed as follows:

$$\begin{cases} \delta_u = \dfrac{U_{me} - U_{re}}{U_{base}} \times 100\% \\ \delta_i = \dfrac{I_{me} - I_{re}}{I_{base}} \times 100\% \end{cases} \tag{10}$$

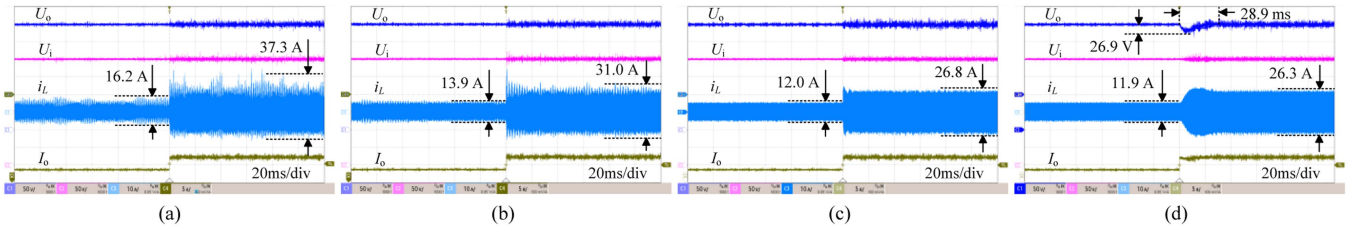

Fig. 6. Experimental results of the transient response for load stepping from 80 to 40 Ω. (a) Conventional MPC. (b) Proposed method with $\beta = 5$. (c) Proposed method with $\beta = 10$. (d) PI control.

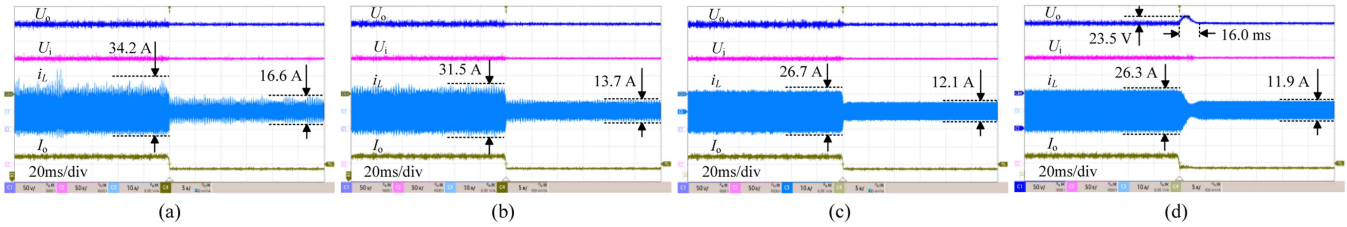

Fig. 7. Experimental results of the transient response for load stepping from 40 to 80 Ω. (a) Conventional MPC. (b) Proposed method with $\beta = 5$. (c) Proposed method with $\beta = 10$. (d) PI control.

TABLE I
MAIN EXPERIMENTAL PARAMETERS

Parameters	Symbols	Values
Switching frequency	f_s	50 kHz
Transformer's turn ratio	n	16:16
Input-side capacitor	C_1	500 μF
Output-side capacitor	C_2	500 μF
Equivalent inductance	L	80 μH
Load resistance	R	80/40 Ω
Input voltage	U_{i}	300 V
Reference output voltage	$U_{\mathrm{o}}^{\mathrm{ref}}$	300 V

where U_{re} and U_{me} represent the measured and real voltage, respectively, I_{re} and I_{me} represent the measured and real current, respectively. U_{base} and I_{base} are voltage rating and current rating. Based on the parameters of the converter in Table I, assuming that the output voltage has reached the reference value at the current moment, Fig. 5 illustrates the relationship between the noise intensity and β in relation to the phase-shift angle under different noise types. It can be seen that under the same noise intensity, the influence of noise on the output voltage is much greater than that of the output current and the input voltage, which explains why the noise influence of the input voltage and the output current can be ignored. When the noise intensity is represented by the red dotted line, it can be noted that an increase in the regulation coefficient β results in a reduction in the fluctuation of the phase-shift angle, which is more effective in tolerating noise, but it can also reduce the dynamic performance. Choosing an appropriate β can well balance the noise tolerance performance and the dynamic performance, which is experimentally presented in Section IV.

B. Static Accuracy Analysis

After introducing the virtual capacitor into the controller, the output voltage prediction model of the DAB converter in the steady state can be obtained as

$$U_{\mathrm{o}}^{*}(k+1) = U_{\mathrm{o}}(k) + \frac{nU_{\mathrm{i}}(k)\beta}{2{f_{\mathrm{s}}}^{2}LC_2}D(1-|D|) - \frac{I_{\mathrm{o}}(k)\beta}{f_{\mathrm{s}}C_2} = U_{\mathrm{o}}^{\mathrm{ref}}. \tag{11}$$

By combining (2), the error between the actual output voltage and the reference value at $k+1$ can be expressed as

$$\Delta U_{\mathrm{o}}(k+1) = U_{\mathrm{o}}^{\mathrm{ref}} - U_{\mathrm{o}}(k+1) = \left[U_{\mathrm{o}}^{\mathrm{ref}} - U_{\mathrm{o}}(k)\right]\frac{\beta-1}{\beta} = \Delta U_{\mathrm{o}}(k)\frac{\beta-1}{\beta}. \tag{12}$$

Similarly, at $k+n$

$$\Delta U_{\mathrm{o}}(k+n) = \Delta U_{\mathrm{o}}(k)\left(\frac{\beta-1}{\beta}\right)^{n}. \tag{13}$$

When n is sufficiently large, $\Delta U_{\mathrm{o}}(k+n)$ approaches zero, which means that the virtual capacitor does not introduce steady-state errors into the system.

IV. EXPERIMENTAL RESULTS

In order to verify the effectiveness of the proposed noise tolerance method, an experimental prototype of the DAB converter is built. The main experimental parameters are given in Table I.

Fig. 6 shows experimental results of the transient response for load stepping from 80 to 40 Ω. Fig. 6(a) shows the conventional results of MPC, Fig. 6(b) and (c) shows the results of MPC for $\beta = 5$ and $\beta = 10$, respectively, Fig. 6(d) shows the transient response under proportional–integral (PI) control. For Fig. 6(a), the experimental results show that the inductor peak current reaches 16.2 A for a resistance of 80 Ω and 37.3 A for a resistance of 40 Ω, indicating constant phase-shift angle jumping between 0 and 0.5. The performance under CCS-MPC is greatly affected

by noise, and stable control cannot be realized. Fig. 6(c) shows that the inductor peak current is only 12.0 and 26.8 A for $\beta = 10$, which are much smaller than the results of conventional MPC. For Fig. 6(d), the experimental results show that the inductor peak current reaches 11.9 and 26.3 A, which is similar to the results of $\beta = 10$. Therefore, our proposed method significantly improves the robustness of the system against ADC noise. The current and voltage ripples can be significantly reduced, and stable control can be realized. Moreover, Fig. 6(d) shows the corresponding dynamic response time under PI control is up to 28.9 ms. In comparison, the MPC with the noise tolerance method reaches a steady state significantly faster than the PI control. Meanwhile, by comparing Fig. 6(b) and (c), it is evident that increasing the regulation coefficient of the virtual capacitor results in better noise tolerance performance, stabilizes the phase-shift angle, and reduces current and voltage ripples.

Fig. 7 compares the dynamic performance for load stepping from 40 to 80 Ω. Fig. 7(a)–(d) shows the transient response under conventional MPC, proposed MPC with $\beta = 5$, 10, and PI control.

In summary, the MPC with the noise tolerance method effectively suppresses the ADC noise impact and maintains rapid dynamic performance, while different β values have little effect on the dynamic response time, clearly outperforming the PI control.

V. Conclusion

DC–DC power converters regulated by duty cycle or phase-shift under continuous control set model predictive control (CCS-MPC) are inevitably impacted by noise. This letter proposes a simple and effective noise tolerance method to address this issue without the need for extra hardware or increased computational burden. The method has been experimentally validated and successfully mitigates the impact of ADC noise on CCS-MPC, while maintaining outstanding dynamic performance. The proposed method represents the best solution thus far.

References

[1] X. Li et al., "Model-predictive control with parameter identification for multi-dual-active-bridge converters achieving accurate power balancing," *IEEE Trans. Power Electron.*, vol. 38, no. 9, pp. 10880–10894, Sep. 2023.

[2] Y. Cai, C. Gu, J. Li, J. Yang, G. Buticchi, and H. Zhang, "Dynamic performance enhancement of a triple active bridge with power decoupling-based configurable model predictive control," *IEEE Trans. Transport. Electrific.*, vol. 9, no. 2, pp. 3338–3349, Jun. 2023.

[3] A. Garcés-Ruiz, S. Riffo, C. González-Castaño, and C. Restrepo, "Model predictive control with stability guarantee for second-order DC/DC converters," *IEEE Trans. Ind. Electron.*, vol. 71, no. 5, pp. 5157–5165, May 2024.

[4] A. A. Ahmed, B. K. Koh, and Y. I. Lee, "A comparison of finite control set and continuous control set model predictive control schemes for speed control of induction motors," *IEEE Trans. Ind. Informat.*, vol. 14, no. 4, pp. 1334–1346, Apr. 2018.

[5] J. Yang, J. Liu, J. Zhang, N. Zhao, Y. Wang, and T. Q. Zheng, "Multirate digital signal processing and noise suppression for dual active bridge DC–DC converters in a power electronic traction transformer," *IEEE Trans. Power Electron.*, vol. 33, no. 12, pp. 10885–10902, Dec. 2018.

[6] Y. Liu, M. Huang, H. Wang, X. Zha, J. Gong, and J. Sun, "Reliability-oriented optimization of the LC filter in a buck DC–DC converter," *IEEE Trans. Power Electron.*, vol. 32, no. 8, pp. 6323–6337, Aug. 2017.

[7] I. Z. Petric, P. Mattavelli, and S. Buso, "Feedback noise propagation in multisampled DC–DC power electronic converters," *IEEE Trans. Power Electron.*, vol. 37, no. 1, pp. 150–161, Jan. 2022.

[8] M. Han, H. He, X. Wang, Z. Dong, and Z. Zhang, "Current-sensorless model predictive control of dual active bridge converters with Kalman filter," in *Proc. IEEE Int. Conf. Predictive Control Elect. Drives Power Electron.*, 2021, pp. 663–667.

[9] Q. Xiao, L. Chen, H. Jia, P. W. Wheeler, and T. Dragičević, "Model predictive control for dual active bridge in naval DC microgrids supplying pulsed power loads featuring fast transition and online transformer current minimization," *IEEE Trans. Ind. Electron.*, vol. 67, no. 6, pp. 5197–5203, Jun. 2020.

[10] H. Peng, A. Prodic, E. Alarcon, and D. Maksimovic, "Modeling of quantization effects in digitally controlled DC–DC converters," *IEEE Trans. Power Electron.*, vol. 22, no. 1, pp. 208–215, Jan. 2007.

[11] S. J. Miller, *The Probability Lifesaver: All the Tools You Need to Understand Chance*. Princeton, NJ, USA: Princeton Univ. Press, 2017.

[12] A. Sangswang, "An experimental study of random noise characteristics in a power converter," in *Proc. IEEE Region 10 Conf.*, 2005, pp. 1–5.